2013-03

Effect of denoising on the quality of reconstructed images in digital breast tomosynthesis

Proceedings of SPIE, Bellingham, v. 8668, 86680C, 2013
http://www.producao.usp.br/handle/BDPI/47646

Effect of Denoising on the Quality of Reconstructed Images in Digital Breast Tomosynthesis

Marcelo A. C. Vieira*[a], Predrag R. Bakic[b], Andrew D. A. Maidment[b]

[a] Department of Electrical Engineering, University of São Paulo, São Carlos, SP, Brazil
[b] Department of Radiology, University of Pennsylvania, Philadelphia, PA, USA

ABSTRACT

Individual projection images in Digital Breast Tomosynthesis (DBT) must be acquired with low levels of radiation, which significantly increases image noise. This work investigates the influence of a denoising algorithm and the Anscombe transformation on the reduction of quantum noise in DBT images. The Anscombe transformation is a variance-stabilizing transformation that converts the signal-dependent quantum noise to an approximately signal-independent Gaussian additive noise. Thus, this transformation allows for the use of conventional denoising algorithms, designed for additive Gaussian noise, on the reduction of quantum noise, by working on the image in the Anscombe domain. In this work, denoising was performed by an adaptive Wiener filter, previously developed for 2D mammography, which was applied to a set of synthetic DBT images generated using a 3D anthropomorphic software breast phantom. Ideal images without noise were also generated in order to provide a ground-truth reference. Denoising was applied separately to DBT projections and to the reconstructed slices. The relative improvement in image quality was assessed using objective image quality metrics, such as peak signal-to-noise ratio (PSNR) and mean structural similarity index (SSIM). Results suggest that denoising works better for tomosynthesis when using the Anscombe transformation and when denoising was applied to each projection image before reconstruction; in this case, an average increase of 9.1 dB in PSNR and 58.3% in SSIM measurements was observed. No significant improvement was observed by using the Anscombe transformation when denoising was applied to reconstructed images, suggesting that the reconstruction algorithm modifies the noise properties of the DBT images.

Keywords: Image denoising, quantum noise, Digital Breast Tomosynthesis, Anscombe transformation, Wiener filter.

1. INTRODUCTION

Digital breast tomosynthesis (DBT) is a relatively new imaging modality for breast cancer screening in which a limited number of low-dose x-ray projections are acquired as the x-ray tube moves over an arc.[1] A 3D volume is then reconstructed from these projections and tomographic slices of the breast are generated. Typically, DBT reconstructions are performed on planes parallel to the breast support at various depths in the breast volume.[2] The advantage over 2D digital mammography is that tomosynthesis can reduce the problems caused by tissue overlap when projecting breast 3D parenchymal structures into a plane.[1,2] Preliminary studies indicate that DBT has greater sensitivity and specificity for cancer detection relative to 2D digital mammography.[3]

There have been a number of studies investigating the effect of tomosynthesis acquisition parameters on image quality.[4,5] Among others, the main factors that affects the quality of the reconstructed slices are the number of projections acquired, scan angle, spatial resolution, dose levels, quantum noise and the choice of reconstruction algorithm. Regarding dose levels, tomosynthesis examination normally is done with a total radiation exposure similar to a conventional mammogram. This means that individual projections are acquired with very low levels of radiation dose, typically about 5-15% of a normal single-view 2D mammography. Thus, low-dose acquisition significantly degrades image quality by increasing the amount of quantum noise.

*mvieira@sc.usp.br; phone +55-16-3373-9353; fax +55-16-3373-9372; www.sel.eesc.usp.br

Medical Imaging 2013: Physics of Medical Imaging, edited by Robert M. Nishikawa, Bruce R. Whiting, Christoph Hoeschen,
Proc. of SPIE Vol. 8668, 86680C · © 2013 SPIE · CCC code: 1605-7422/13/$18 · doi: 10.1117/12.2007804

In previous work,[6,7] we presented a denoising algorithm for 2D digital mammography based upon a fully adaptive Wiener filter, which reduces image noise without significantly affecting image sharpness. Additionally, we proposed the use of the Anscombe transformation[8-10] to stabilize the noise variance before applying the denoising filter, providing better reduction of quantum noise in digital mammography. The present work investigates how quantum noise in low dose DBT projections influences the quality of the reconstructed slices and how it would be altered if our denoising algorithm were to be applied either before or after the tomographic reconstruction. The use of the Anscombe transformation before denoising has also been investigated in order to stabilize the noise variance.

2. METHODOLOGY

2.1 Adaptive Wiener filtering

The following simple model can be considered to describe the noise-degradation process during image acquisition, considering an additive white noise.

$$g(x,y) = f(x,y) + n(x,y)\,, \tag{1}$$

where $g(x,y)$ is the degraded (noisy) image, $f(x,y)$ is the input image and $n(x,y)$ is the additive noise, all at coordinates *x* and *y*. Denoising techniques usually manipulate this equation to obtain an estimate, $\hat{f}(x,y)$, of the input image when $g(x,y)$ and $n(x,y)$ are known.

The Wiener filter calculates an estimate, $\hat{f}(x,y)$, of the expected noise-free image that minimizes the mean squared error. Specifically, when noisy image $g(x,y)$ is assumed to have a Gaussian additive noise, the Wiener filter is the optimal filter and is expressed as follows:[7]

$$\hat{f}(x,y) = \bar{f}(x,y) + \frac{\sigma_f^2(x,y)}{\sigma_f^2(x,y)+\sigma_n^2(x,y)}\left[g(x,y) - \bar{g}(x,y)\right], \tag{2}$$

where $\bar{f}(x,y)$ and $\sigma_f^2(x,y)$ are the mean and variance of the input image, respectively; $\bar{g}(x,y)$ is the mean of the noisy image $g(x,y)$; and $\sigma_n^2(x,y)$ is the variance of the noise.

Parameters $\bar{f}(x,y)$ and $\sigma_f^2(x,y)$ should estimated considering local statistics within a small neighborhood around the pixel being processed.[6,7] As the input image, $f(x,y)$, is not known, these parameters should be estimated by blurring the noisy image $g(x,y)$ with a low-pass filter, which produced a preliminary estimate of the input image, denoted by $\hat{\hat{f}}(x,y)$. In this work, we used a 3×3 averaging filter mask on $g(x,y)$ to obtain $\hat{\hat{f}}(x,y)$. Thus, denoting the neighborhood around $\hat{\hat{f}}(x,y)$ by A_{ij}, the local mean and variance of $\hat{\hat{f}}(x,y)$ were calculated by:

$$\bar{\hat{f}}(x,y) = \frac{1}{M^2}\sum_{i=0}^{M-1}\sum_{j=0}^{M-1}\hat{\hat{f}}\,(i,j)\,, \quad i,j \in A_{ij} \tag{3}$$

$$\hat{\hat{\sigma}}_f^2(x,y) = \frac{1}{M^2}\sum_{i=0}^{M-1}\sum_{j=0}^{M-1}[\hat{\hat{f}}\,(i,j) - \bar{f}(i,j)]^2\,, \quad i,j \in A_{ij} \tag{4}$$

where *M* denotes the size of the square neighborhood A_{ij}.

The choice of the size *M* for local mean and variance estimation is crucial and has a great impact on the performance of the filter[7]. The bigger the area of the neighborhood, the more noise that will be removed, but also the restored image will be more blurred. Thus, to properly define the size of the neighborhood A_{ij}, we considered the method originally proposed by Rabbani[11], where *M* is automatically adjusted depending on the signal activity relative to the noise activity within the neighborhood A_{ij}. Initially, the area A_{ij} is chosen to be a 5 × 5 square neighborhood around the pixel at coordinates *(x,y)* which is being processed (*M* = 5). In that region, we measured the relative signal activity, $\alpha(x,y)$, which is defined as:

$$\alpha(x,y) = \frac{\hat{\sigma}_f^2(i,j)}{\sigma_g^2(i,j)}, \qquad i,j \in A_{ij} \tag{5}$$

where $\hat{\sigma}_f^2(x,y)$ is the variance of the preliminary estimate of the input image (Eq. 4) and $\sigma_g^2(i,j)$ is the variance of the noisy image, both measured within the 5 × 5 neighborhood A_{ij} around the pixel being processed.

The parameter $\alpha(x,y)$ is in the range [0,1] and denotes a relative measure of the signal activity (variance) versus the noise variance.[7,11] Values of $\alpha(x,y)$ close to zero correspond to flat areas, with little signal variation compared to the noise variance. Conversely, values of $\alpha(x,y)$ close to one imply that the signal variance dominates the noise variance and are indicative of areas with fine details or sharp transitions. Thus, the size *M* of the square neighborhood around the pixel being processed is chosen depending on the value of $\alpha(x,y)$ considering the following criteria: if $0.2 < \alpha(x,y) < 0.6$, moderate signal activity is present and the required statistics are estimated from a 5 × 5 neighborhood using Eq. (3) and Eq.(4). If $\alpha(x,y) < 0.2$, a relatively flat area is detected and the size of the square neighborhood is increased to 7 × 7 to enclose more pixels and to more effectively average out the noise. Finally, if $\alpha(x,y) > 0.6$, a possible sharp transition area has been encountered, and a set of gradient operations are performed on the pixels in the 5 × 5 neighborhood to detect the gradient orientation. Then, this area is divided into two sub-regions and we consider only the sub-region on the side of the sharp transition with an average value more similar to the pixel being processed.[7,11] Figure 1 summarizes the criteria used to select the size *M* of the square neighborhood around the pixel being processed. The local mean and variance computed using this algorithm allowed the Wiener filter to reduce image noise without significantly affecting image sharpness.[6,7]

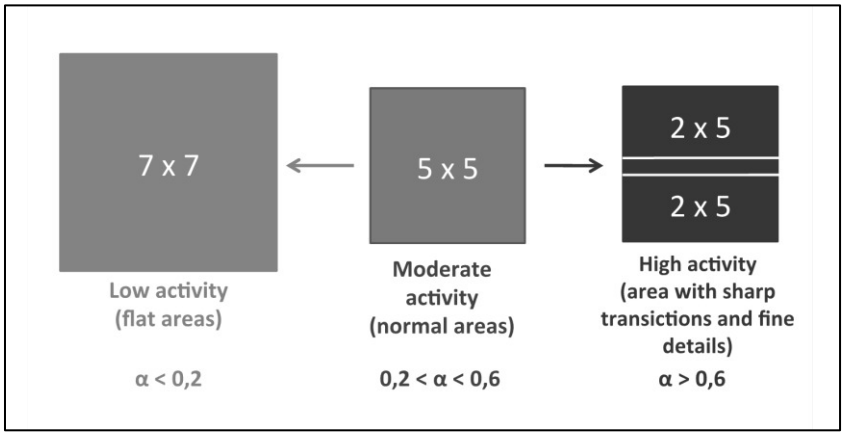

Figure 1 – Summary of the method used to properly choose the size *M* of the square neighborhood to estimate local mean and variance to Wiener filtering.

2.2 Anscombe transformation

The Anscombe transformation is a variance-stabilizing transformation that converts a random variable with a Poisson distribution into a variable with an approximately additive, signal-independent Gaussian distribution with zero mean and unity variance.[8-10] The Anscombe transformation of degraded image $g(x,y)$ is given by the following:[8]

$$z(x,y) = 2\sqrt{g(x,y) + \frac{3}{8}}\ , \tag{6}$$

This equation can be represented by the following additive model:[9]

$$z(x,y) = \left(2\sqrt{r(x,y) + \frac{1}{8}}\right) + v(x,y) = s(x,y) + v(x,y)\ , \tag{7}$$

where $r(x,y)$ is the expected value (rate) of the Poisson-distributed image and $v(x,y)$ is the additive term, which is independent of the signal $s(x,y)$ and has an approximately Gaussian distribution.[9]

After the Anscombe transformation, the additive term $v(x,y)$ includes both the quantum noise converted into Gaussian noise and the electronic white noise, originally incorporated by the digitization process. Thus, this transformation allows for the use of any conventional denoising technique to remove additive Gaussian white noise by acting on the image $z(x,y)$ in the Anscombe domain.[7] Typically, the removal of Poisson noise using the Anscombe transformation is performed through the following three-steps:[10] First, the noise variance is stabilized by applying the Anscombe transformation to the noisy image, producing a signal in which the noise can be treated as additive Gaussian with unitary variance. Second, the noise is removed using a conventional denoising algorithm for additive Gaussian white noise. Third, an inverse transformation is applied to the denoised signal, obtaining the estimate of the signal of interest.

In this work, we used the adaptive Wiener filter presented in Eq. (2) to obtain an estimate, $\hat{s}(x,y)$, of the mammographic image in the Anscombe domain. After the Anscombe transformation we can assume that $\sigma_v^2(x,y) = 1$. Moreover, $\bar{s}(x,y)$ is equal to $\bar{z}(x,y)$ because the mean of the noise, $\bar{v}(x,y)$, is equal to zero after Anscombe transformation. Thus, denoising in the Anscombe domain simplifies Eq. (4), which can be rewritten as follows:[7]

$$\hat{s}(x,y) = \bar{z}(x,y) + \frac{\sigma_s^2(x,y)}{\sigma_s^2(x,y)+1}[z(x,y) - \bar{z}(x,y)]\ , \tag{8}$$

where $\bar{z}(x,y)$ is the mean of the image and $\sigma_s^2(x,y)$ is the variance of the signal (or an estimate of the signal) in the Anscombe domain.

After the filtering procedure, the inverse Anscombe transformation must be applied to obtain the estimate, $\hat{r}(x,y)$, of an approximately noise-free mammographic image in the spatial domain. The inverse Anscombe transformation is described by [7]

$$\hat{f}(x,y) = \frac{1}{4}\hat{s}(x,y)^2 - \frac{1}{8}\,. \tag{9}$$

2.3 Anthropomorphic software breast phantom

In order to evaluate the denoising methodology, a set of synthetic DBT projections was generated using a 3D anthropomorphic breast software phantom, developed previously. The phantom design is based upon a detailed analysis of breast anatomy visualized by clinical imaging and sub-gross pathology provided realistic simulation of the breast.[12-16] This software phantom is able to simulate 3D breast models with skin, regions of adipose and fibroglandular tissue, and the matrix of Cooper's ligaments and adipose compartments. The adipose compartments are simulated using a seeded region-growing algorithm where compartments are grown from a set of seed points with specific orientation and growing speed. Simulation parameters could be selected to cover the breadth of variations in breast anatomy observed clinically.

Using this software, we created nine different 3D breast models with different volume, grandularity and adipose compartment distribution, simulating several different anatomic noise patterns. A cluster of microcalcifications of approximately 15 cm^3 (2.5 × 2.5 × 2.5 cm) was embedded within each one of these phantoms at random locations (position and depth).

An image database containing DBT projections of all phantoms was generated using the acquisition geometry which corresponds to a GE DBT prototype system (Senographe DS, General Electric Healthcare, Chalfont St. Giles, U.K.).[14] Each phantom was deformed to model mammographic compression, based upon a finite element model of 50% reduction in compressed phantom thickness.[15] Fifteen DBT low-dose projections were generated for each phantom considering an angular range of approximately ±20.0 degrees and quantum noise levels representative of a case of normal clinical dose. An anti-scatter grid was not simulated. Reference projections images without noise were also generated in order to provide ground-truth information, which allowed the evaluation of the denoising performance using objective signal fidelity measurements.[17,18] Thus, a total of 270 projections images were generated, each one with 1920 × 2304 pixels, 14 bits and a pixel size of 100 μm. Only the mediolateral-oblique (MLO) view was considered for this study. Figure 2 shows examples of synthetic DBT central projections (acquisition angle = 0°) of three different 3D phantom models. The white arrows indicate the location of the microcalcification cluster.

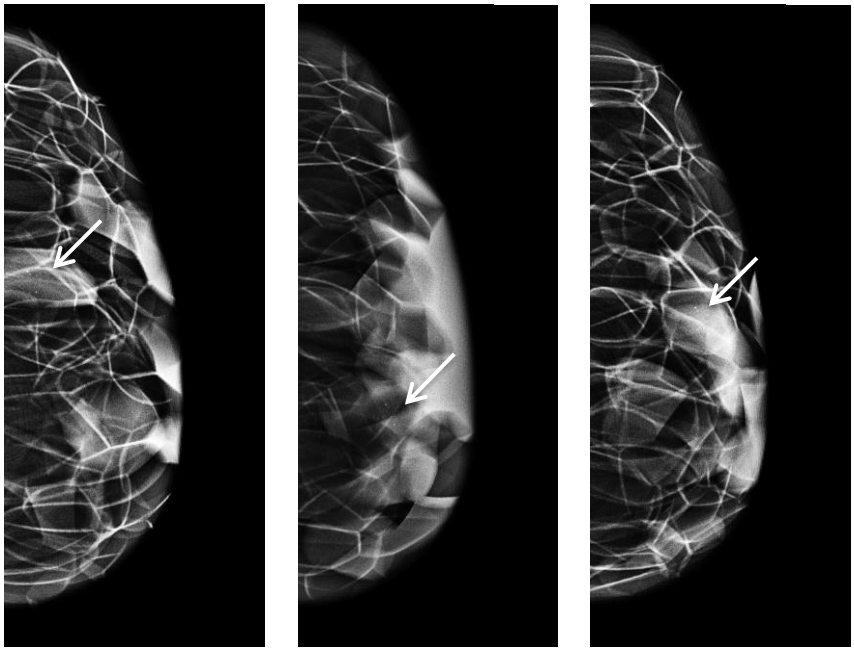

Figure 2 – Examples of synthetic DBT images (central projections) of three different 3D phantom models with different internal composition used for denoising evaluation. The white arrows indicate the location of the microcalcification cluster.

Tomographic slices were generated from synthetic projections using a commercial DBT reconstruction software[19] (Briona™ 3D, Real-Time Tomography, LLC, Villanova, PA). This software uses a filtered back projection algorithm to generate reconstructed slices on planes parallel to the breast support at various depths of the breast volume. For this study, we generated slices 0.5 mm thick on a slice spacing of 0.5 mm. Figure 3 shows examples of tomographic reconstructed slices generated from the synthetic DBT projections of three different 3D phantom models. The white arrows indicate the location of the microcalcification cluster.

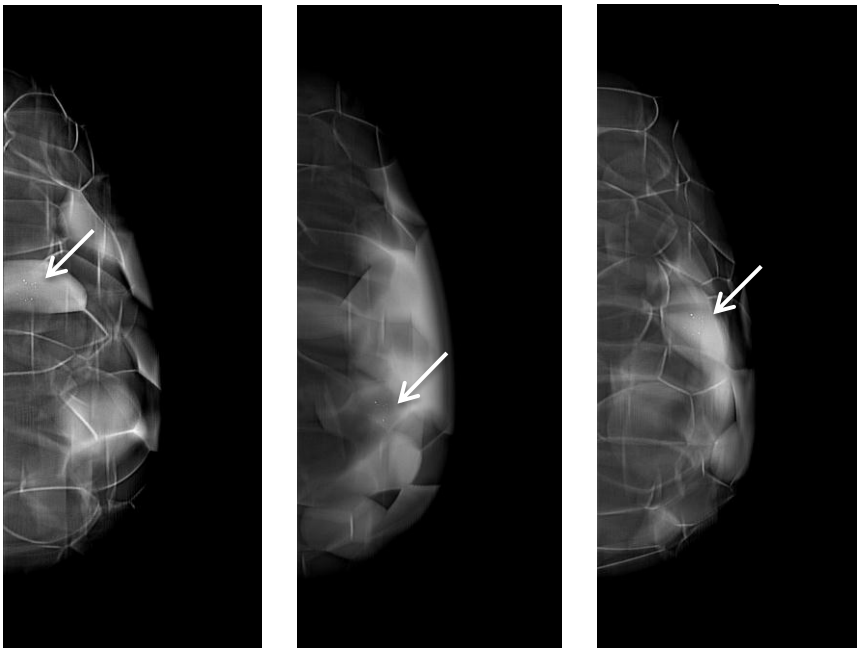

Figure 3 – Examples of three images of DBT reconstructed slices generated by filtered back projecting the synthetic DBT projections using Briona™ 3D reconstruction software (Real-Time Tomography, LLC, Villanova, PA). The white arrows indicate the location of the microcalcification cluster.

2.4 Evaluation of denoising performance

The evaluation of denoising performance was conducted using objective image quality metrics. These measurements was made considering images denoised by using the adaptive Wiener filter in the spatial domain and also in the Anscombe domain, in order to evaluate the improvement on quantum noise reduction achieved when using the Anscombe transformation. Objective measurements was performed by the calculation of signal-fidelity measures, which compare two signals by providing a quantitative score that describes the degree of similarity between them.[17] These measurements was only possible in this work because we generated synthetic images from a breast phantom model. In this case, we compared the denoised image obtained with or without the Anscombe transformation to the ideal image (reference) provided by generating DBT projections without noise using the breast phantom model.

In order to perform an objective assessment of the denoising methodology, we calculated the following signal-fidelity parameters: peak of signal-to-noise ratio (PSNR)[17] and structural similarity index (SSIM).[18] The PSNR represents the ratio between the maximum possible power of a signal and the power of the corrupting noise that affects the fidelity of its representation. Typically, the PSNR value is given in decibels (dB) and a higher PSNR would normally indicate denoising of higher quality.[17] The SSIM index includes human visual perception in the measurement by extracting information about the luminance, contrast and structure of an image. It was designed to improve traditional signal-fidelity measures.[18] SSIM is calculated on various windows of both denoised and reference images, which should be displaced pixel-by-pixel in both images. In practice, the mean value of the SSIM indexes (MSSIM) of all windows is used to evaluate the overall image quality. The resultant MSSIM index is a decimal value between -1 and 1, where a value of 1 can be reached only in the case of two identical images.[18]

In this work, denoising was applied to all DBT synthetic images considering three different approaches (Figure 4):

1. **Study 1**: denoising was applied to all the projection images and the performance was assessed using the projections. No reconstruction was performed in this case.
2. **Study 2**: denoising was applied to all the projection images but the denoising performance was assessed using the slices generated after reconstruction.

3. **Study 3**: denoising was applied to the reconstructed slices and the performance was assessed using the slices generated after reconstruction.

Figure 4 summarizes the different approaches using to evaluate the performance of the denoising algorithm and the Anscombe transformation on the improvement of DBT images.

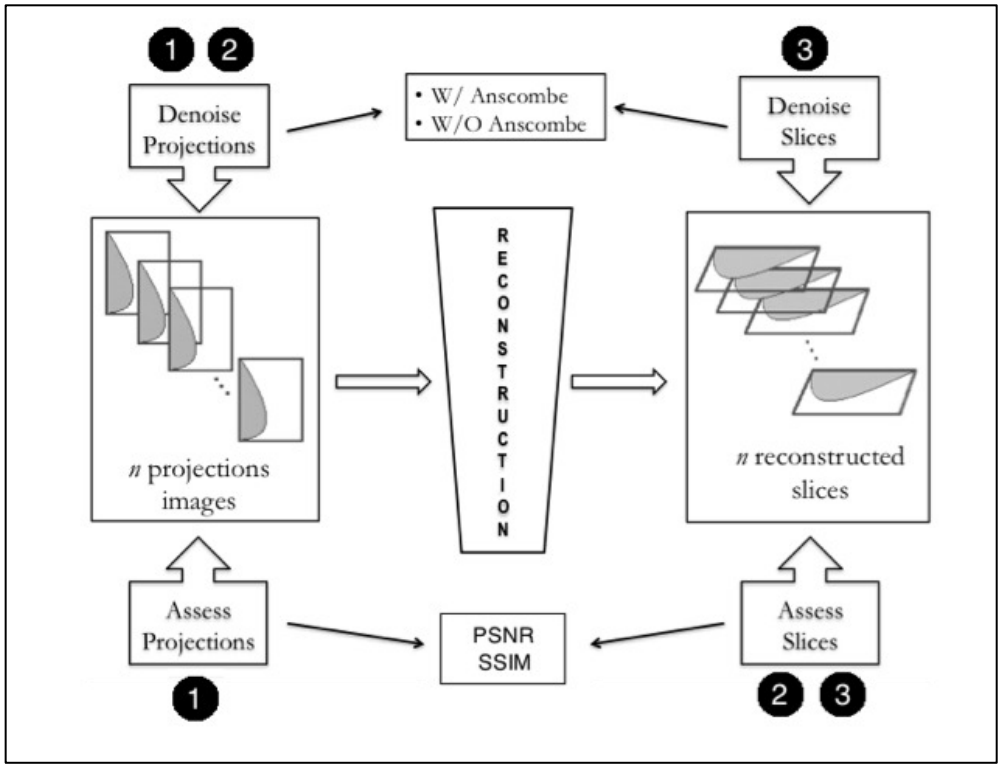

Figure 4 – Summary of the methodology used to evaluate the effect of denoising in DBT. (1) Denoising and assessment was applied to the projections; (2) Denoising was applied to the projections but the assessment was performed in the reconstructed slices; (3) Denoising and assessment was applied to the reconstructed slices.

3. RESULTS

3.1 Study 1 – Denoise projections – Assess projections

Results of each approach conducted in order to apply denoising in DBT images (studies 1, 2, and 3) will be presented separately. First, we show one example of images obtained when the denoising and the assessment was applied to the projections (Study 1). Figure 5 shows a region of interest (ROI) of size 256×256 pixels, which includes the microcalcification cluster, extracted from the central projection of one of the synthetic images used in this work. Image on the left (a) shows the original (noisy) image; image (b) is the noiseless image used as a reference (ground-truth); (c) is the denoised image obtained when the Wiener filter was applied in the spatial domain, without using Anscombe transformation and (d) is the denoised image obtained when the Anscombe transformation was used before applying the Wiener filter.

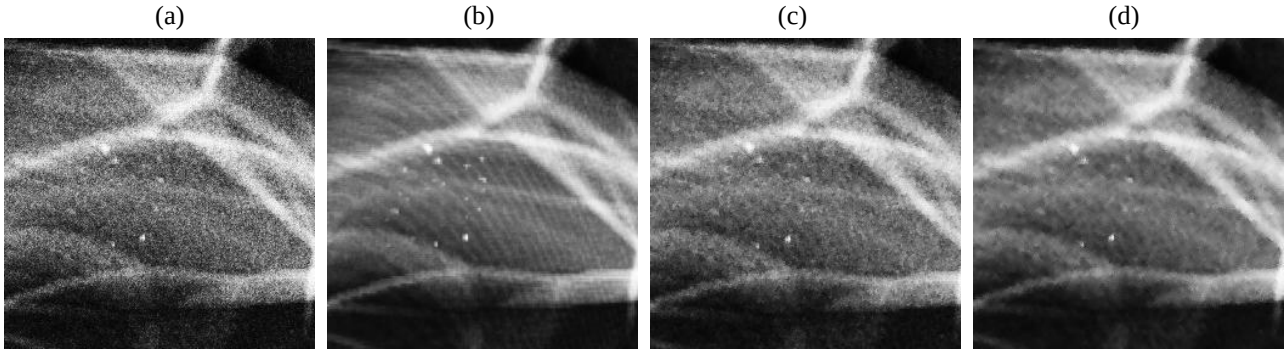

Figure 5 – Study 1: results of denoising DBT projections and assess DBT projections: (a) original (noisy) image; (b) noiseless image used as a reference (ground-truth); (c) denoised image obtained when the Wiener filter was applied in the spatial domain, without using Anscombe transformation; (d) denoised image obtained when the Anscombe transformation was used before applying the Wiener filter.

Images presented in Figure 5 show that the use of Anscombe transformation notably improved noise reduction achievable with Wiener filtering (Figure 5d). The adaptive filtering preserved the fine details and sharp transitions in the image, even for an image corrupted by a high level of quantum noise.

Objective image quality metrics calculated for DBT projections (Study 1) are presented in Figure 6. The graphs show the mean values and the standard deviation of PSNR and SSIM measurements calculated for each phantom before and after denoising by using the Wiener filter applied with and without the Anscombe transformation. Values were calculated considering 15 ROIs of size 256 × 256 pixels that include the microcalcification cluster (as shown in Figure 5) extracted from all projections of each one of the phantoms: one ROI of each projection.

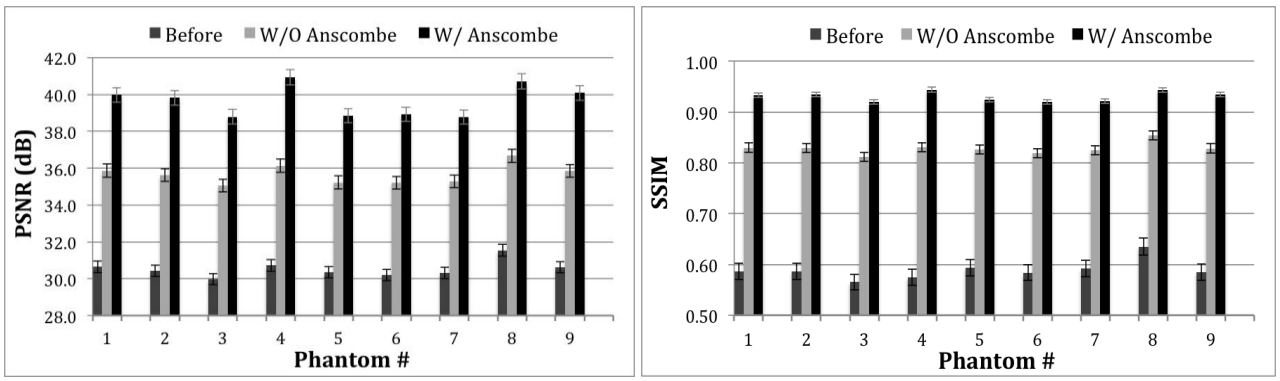

Figure 6 – Study 1: PSNR (left) and SSIM (right) mean values and the correspondent standard deviation measured for 15 ROIs of size 256 × 256 pixels which include the microcalcification cluster extracted from all projections of each one of the phantoms: one ROI of each projection. Values were calculated before and after denoising by using the Wiener filter applied with and without the Anscombe transformation.

The average values and the standard deviation of PSNR and SSIM measurements of all ROIs extracted from the projections images of all 9 phantoms are shown in Table 1 (n = 15 projections × 9 phantoms = 135 images). The relative improvement in image quality provided by using or not the Anscombe transformation was also calculated. Paired two-tailed Student´s t-test was used to evaluate if the improvement on image quality by using the denoising filter and by using the Anscombe transformation is statistically significant.

Table 1. Study 1: average values and the standard deviation of PSNR and SSIM measurements calculated for all projections images of all phantoms (135 ROIs). Values were calculated before and after denoising by using the Wiener filter applied with and without the Anscombe transformation.

Denoising Method	PSNR (dB)				SSIM			
	Before Denoising	After Denoising	Relative improvement (dB)	*p* value	Before Denoising	After Denoising	Relative improvement (%)	*p* value
W/O Anscombe	30.53 ± 0.34	35.65 ± 0.35	5.12 ± 0.06	< 0.0001	0.589 ± 0.02	0.828 ± 0.01	40.78 ± 2.11	< 0.0001
W/ Anscombe	30.53 ± 0.34	39.65 ± 0.36	9.12 ± 0.11	< 0.0001	0.589 ± 0.02	0.931 ± 0.01	58.25 ± 3.34	< 0.0001
PSNR improvement using Anscombe transformation (dB)			4.00 ± 0.10	< 0.0001	**SSIM improvement using Anscombe transformation (%)**		17.47 ± 1.25	< 0.0001

We observed through Table 1 that the Wiener filter achieved much better noise reduction when applied in the Anscombe domain; an average increase of 9.12 dB in the PSNR measurements was observed when denoising was applied in the Anscombe domain versus an average increase of 5.12 dB when denoising was applied in the spatial domain (w/o Anscombe), showing an increase of 4.00 dB in the image quality when using the Anscombe transformation. The same behavior was observed for the SSIM index, which increased 17.47% more when the Anscombe transformation was used.

3.2 Study 2 – Denoise projections – Assess slices

Figure 7 shows one example reconstructed slice (0.5 mm thick) generated by using denoised projections (Study 2), i.e., denoising was applied to all projections (before reconstruction), but the image quality assessment was done considering the resulted slices (after reconstruction). A ROI of size 256 × 256 pixels, which includes the microcalcification cluster, was extracted from one of the slices generated by reconstructing synthetic projection images of one of the phantoms. Image on the left (a) shows the original (noisy) image; image (b) is the noiseless image used as a reference (ground-truth); (c) is the denoised image generated when the Wiener filter was applied in the projections without using Anscombe transformation and (d) is the denoised image generated when the Anscombe transformation was used before applying the Wiener filter to the projections.

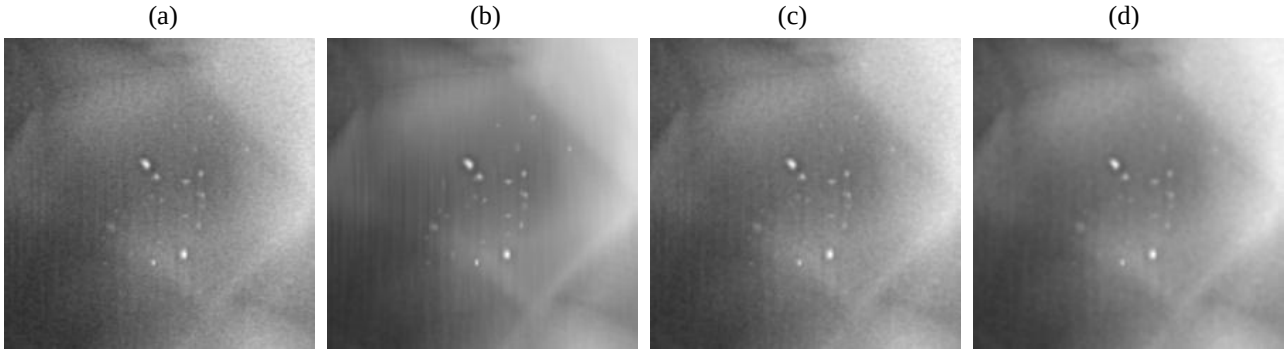

Figure 7 – Study 2: results of DBT reconstructed slices when the denoising was applied to all DBT projections before reconstruction: (a) original (noisy) image; (b) noiseless image used as a reference (ground-truth); (c) denoised image obtained when the Wiener filter was applied to the projections in the spatial domain, without using Anscombe transformation; (d) denoised image obtained when the Anscombe transformation was used before applying the Wiener filter to the projections.

Images presented in Figure 7 show that even after reconstruction the improvement in noise reduction by using the Anscombe transformation is still perceptible (Figure 7d). Objective image quality metrics were also calculated for DBT slices (Study 2) and are presented in Figure 8. The graphs show the mean values and the standard deviation of PSNR and SSIM measurements calculated for each phantom after reconstruction by using original and denoised projections. Values were calculated considering 7 ROIs of size 256 × 256 pixels (as shown in Figure 7) extracted from 7 slices of each one of the phantoms: one ROI of each slice. Slices were selected considering a center slice where the microcalcification cluster was on focus plus three slices below and three slices above this one, considering a step of 0.5 mm.

The average values and the standard deviation of PSNR and SSIM measurements of all ROIs extracted from the reconstructed slices of all 9 phantoms are shown in Table 2 (n = 7 slices × 9 phantoms = 63 images). The relative improvement in image quality provided by using or not using the Anscombe transformation was also calculated. Again, paired two-tailed Student´s t-test was used to evaluate if the improvement on the quality of the reconstructed slices by using the denoising filter and the Anscombe transformation is statistically significant.

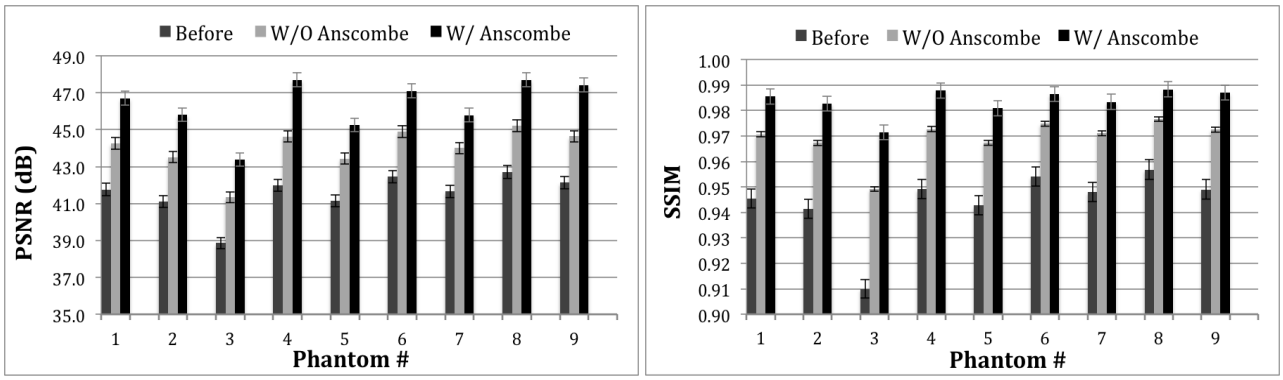

Figure 8 – Study 2: PSNR (left) and SSIM (right) mean values and the correspondent standard deviation measured for 7 ROIs of size 256 × 256 pixels extracted from 7 tomographic slices (0.5 mm thick) of each one of the phantoms: one ROI of each slice. Slices were selected considering a center slice where the microcalcification cluster was on focus plus three slices below and three slices above this one, considering a step of 0.5 mm. Values were calculated before and after denoising by using the Wiener filter applied to the projections (before reconstruction) with and without using the Anscombe transformation.

Table 2. Study 2: average values and the standard deviation of PSNR and SSIM measurements calculated for selected reconstructed slices of all phantoms (63 ROIs). Values were calculated before and after denoising by using the Wiener filter applied with and without the Anscombe transformation.

Denoising Method	**PSNR (dB)**				**SSIM**			
	Before Denoising	**After Denoising**	**Relative improvement (dB)**	***p* value**	**Before Denoising**	**After Denoising**	**Relative improvement (%)**	***p* value**
W/O Anscombe	41.54 ± 0.39	44.00 ± 0.38	2.46 ± 0.02	< 0.0001	0.944 ± 0.004	0.969 ± 0.002	2.66 ± 0.21	< 0.0001
W/ Anscombe	41.54 ± 0.39	46.32 ± 0.32	4.78 ± 0.13	< 0.0001	0.944 ± 0.004	0.983 ± 0.001	4.21 ± 0.35	< 0.0001
PSNR improvement using Anscombe transformation (dB)			2.33 ± 0.11	< 0.0001	**SSIM improvement using Anscombe transformation (%)**		1.55 ± 0.15	< 0.0001

As expected, we observed through Table 2 that the quality of the reconstructed slice is far better than the quality of each individual projection before reconstruction. Before applying denoising, mean value of PSNR for the original projections was 30.53 dB and the SSIM index was 0.589 (Table 1); after reconstruction, mean value of PSNR for the slices was improved to 41.54 dB and SSIM index was improved to 0.944 (Table 2). Regarding the effect of denoising, data in Table 2 show that the quality of reconstructed slices is still better when the projections were denoised in the Anscombe domain; an average increase of 4.78 dB in the PSNR measurements when denoising was applied to projections in the Anscombe domain versus an average increase of 2.46 dB when denoising was applied in the spatial domain (w/o Anscombe), showing and increase of 2.33 dB in the image quality when using the Anscombe transformation before reconstruction. However, the effect of denoising is more perceptible when the assessment was performed on the projections than on the slices, because the quality of the original image (noisy) is worst when considering only the projections as the reconstruction algorithm improves the image quality. Moreover, the same behavior was observed for the SSIM index, which increased only 1.55% more for the slices when the Anscombe transformation was used before reconstruction.

3.3 Study 3 – Denoising slices – Assess slices

The last study (Study 3) was performed applying denoising after reconstruction, i.e., tomographic slices were generated by using noisy (original) projections and denoising was applied to the reconstructed slices, using the Wiener filter with and without Anscombe transformation. Figure 9 shows one example when the denoising was applied after reconstruction. A ROI of size 256 × 256 pixels that includes the microcalcification cluster was extracted from one of the slices generated by reconstructing synthetic projection images of one of the phantoms. Image on the left (a) shows the original (noisy) image; image (b) is the noiseless image used as a reference (ground-truth); (c) is the denoised image generated when the Wiener filter was applied to the slices (after reconstruction) without using Anscombe transformation and (d) is the denoised image generated when the Anscombe transformation was used.

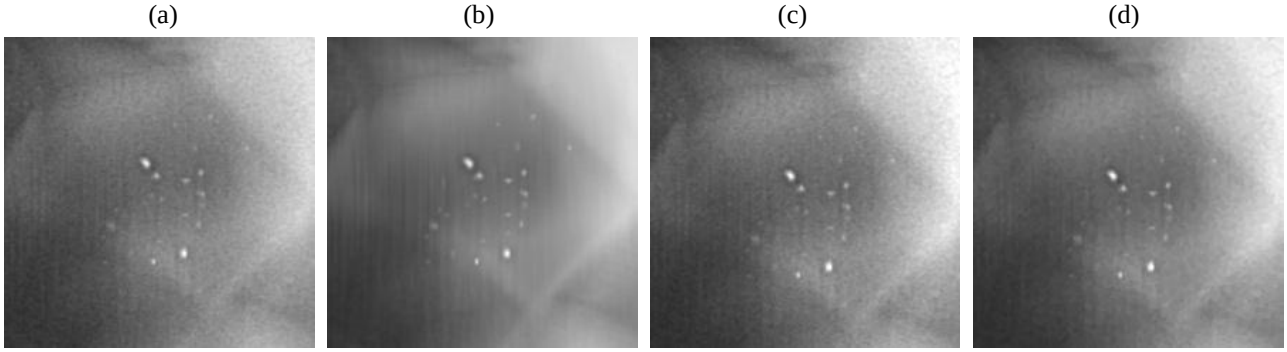

Figure 9 – Study 3: results of DBT reconstructed slices when the denoising was applied after reconstruction: (a) original (noisy) image; (b) noiseless image used as a reference (ground-truth); (c) denoised image obtained when the Wiener filter was applied to the slices in the spatial domain, without using Anscombe transformation; (d) denoised image obtained when the Anscombe transformation was used.

Analyzing the images presented in Figure 9 we noticed that the Anscombe transformation did not influence the performance of the denoising filter after reconstruction. In this case, there was no improvement in noise reduction by using the Anscombe transformation (Figures 9c and 9d). Objective image quality metrics were calculated for DBT slices in this case (Study 3) and are presented in Figure 10. The graphs show the mean values and the standard deviation of PSNR and SSIM measurements calculated for each phantom after reconstruction, before and after denoising. Values were calculated considering 7 ROIs of size 256 × 256 pixels extracted from 7 slices of each one of the phantoms: one ROI of each slice. Slices were selected considering a center slice where the microcalcification cluster was on focus plus three slices below and three slices above this one, considering a step of 0.5 mm.

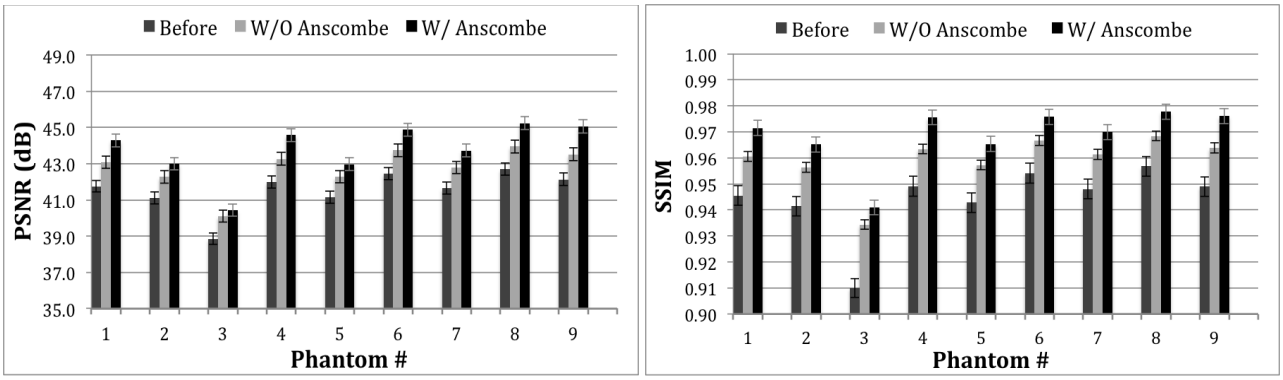

Figure 10 – Study 3: PSNR (left) and SSIM (right) mean values and the correspondent standard deviation measured for 7 ROIs of size 256 × 256 pixels extracted from 7 tomographic slices (0.5 mm thick) of each one of the phantoms: one ROI of each slice. Slices were selected considering a center slice where the microcalcification cluster was on focus plus three slices below and three slices above this one, considering a step of 0.5 mm. Values were calculated before and after denoising by using the Wiener filter to the slices, after reconstruction, with and without using the Anscombe transformation.

The average values and the standard deviation of PSNR and SSIM measurements of all ROIs extracted from the reconstructed slices of all 9 phantoms are shown in Table 3 (n = 7 slices × 9 phantoms = 63 images). The relative improvement in image quality provided by using or not using the Anscombe transformation after the reconstruction was also calculated. Again, paired two-tailed Student´s t-test was used to evaluate if the improvement on the quality of the reconstructed slices by using the denoising filter and the Anscombe transformation is statistically significant.

Table 3. Study 3: average values and the standard deviation of PSNR and SSIM measurements calculated for selected reconstructed slices of all phantoms (63 ROIs). Values were calculated before and after denoising by using the Wiener filter applied with and without the Anscombe transformation.

Denoising Method	PSNR (dB)				SSIM			
	Before Denoising	After Denoising	Relative improvement (dB)	*p* value	Before Denoising	After Denoising	Relative improvement (%)	*p* value
W/O Anscombe	41.54 ± 0.39	42.78 ± 0.38	1.24 ± 0.02	< 0.0001	0.944 ± 0.004	0.959 ± 0.003	1.60 ± 0.13	< 0.0001
W/ Anscombe	41.54 ± 0.39	43.80 ± 0.02	2.26 ± 0.02	< 0.0001	0.944 ± 0.004	0.969 ± 0.002	2.61 ± 0.21	< 0.0001
PSNR improvement using Anscombe transformation (dB)			1.02 ± 0.02	< 0.0001	**SSIM improvement using Anscombe transformation (%)**		1.01 ± 0.08	< 0.0001

In this case (Study 3), we observed through Table 3 that the performance of denoising after reconstruction is worst than in the case that the denoising was applied to the projections before the reconstruction. Data in Table 3 show that the quality of reconstructed slices after denoising improved only slightly (1.24 dB on PSNR w/o Anscombe and 2.26 dB w/ Anscombe and 1.6% on SSIM w/o Anscombe and 2.61% w/ Anscombe). Moreover, the Anscombe transformation increased the performance of our filter by only 1.02 dB for PSNR and 1.01% for SSIM.

4. CONCLUSIONS

In this work we investigated the use of the Anscombe transformation and the adaptive Wiener filter for denoising of DBT images. Denoising was applied separately to the projections (before reconstruction) and to the tomographic slices (after reconstruction). Moreover, we investigated the use of the Anscombe transformation to convert the Poisson noise into Gaussian noise before applying the denoising filter.

Improvements in DBT image quality resulting from the denoising method were evaluated considering objective measurements (PSNR and SSIM). Results suggested that denoising using our adaptive Wiener filter worked better for tomosynthesis when applied in each projection image before reconstruction. Moreover, the use of the Anscombe transformation improved the performance of our denoising filter in about 4.00 dB considering PSNR measurements. It means that the dominant noise in DBT projections is Poisson distributed which was better removed in the Anscombe domain. However, no significant improvement was reported when the Anscombe transformation was applied for denoising reconstructed slices, suggesting that after reconstruction, noise characteristics of the tomographic slices is not Poisson distributed because the filtered backprojection changed the nature of the noise of the DBT projections.

Some of the limitations of this paper and future directions are now addressed. One limitation is that all DBT images used in this study are synthetic images. We chose to use synthetic images because such images provide ground-truth information (noiseless images), which allowed us to use signal-fidelity measurements to calculate objective data about the benefits of using denoising and Anscombe transformation to DBT imaging. Although our synthetic images were acquired by a 3D anthropomorphic breast phantom model and can provide realistic simulation of the breast, a further study using clinical DBT data must be conducted to properly evaluate the benefits of denoising in the quality of DBT imaging.

ACKNOWLEDGEMENTS

The authors would like to thank FAPESP and CNPq for their financial support and Ms. Susan Ng from Real-Time Tomography, LLC (Villanova, PA) for providing us the Briona™ 3D reconstruction software to generate all tomographic slices used in this study.

REFERENCES

[1] Reiser, I. and Nishikawa R. M. “Task-based assessment of breast tomosynthesis: Effect of acquisition parameters and quantum noise”. Med. Phys. 37(4), 1591-1600 (2010).

[2] Acciavatti, R. J. and Maidment, A. D. A. “Observation of super-resolution in digital breast tomosynthesis”. Med. Phys. 39(12), 7518-7539 (2012).

[3] Rafferty, E. A., Park, J. M., Philpotts, L. E., Poplack, S. P., Sumkin, J. H., Halpern, E. F., Niklason, L. T. “Assessing Radiologist Performance Using Combined Digital Mammography and Breast Tomosynthesis Compared with Digital Mammography Alone: Results of a Multicenter, Multireader Trial”. Radiology 266(1), 104-113 (2013).

[4] Mertelmeier, T., Ludwig, J., Zhao B. and Zhao W. “Optimization of Tomosynthesis Acquisition Parameters: Angular Range and Number of Projections”, Lecture Notes in Computer Science 5116, 220-227 (2008).

[5] Deller, T., Jabri, K. N., Sabol, J. M., Ni, X., Avinash, G., Saunders, R. and Uppaluri, R. “Effect of acquisition parameters on image quality in digital tomosynthesis”, Proc. SPIE 6510, 65101L (2007).

[6] Vieira, M. A. C., Bakic, P. R., Maidment, A. D. A., Schiabel, H.; Mascarenhas, N. D. A. “Filtering of Poisson Noise in Digital Mammography Using Local Statistics and Adaptive Wiener Filter”. Proceedings of 11th International Workshop on Breast Imaging, LNCS7361, 268-275 (2012).

[7] Romualdo, L. C. S.; Vieira, M. A. C.; Schiabel, H.; Mascarenhas, N. D. A.; Borges, L.R. “Mammographic image denoising and enhancement using the Anscombe transformation, adaptive Wiener filtering and the modulation transfer function”, Journal of Digital Imaging (online), (2012).

[8] Anscombe, F. J. “The transformation of Poisson, binomial and negative-binomial data”. Biometrika 35, 246-254 (1948).

[9] Mascarenhas, N. D. A., Santos, C. A. N., Cruvinel, P. E. “Transmission tomography under poisson noise using the Anscombe transformation and Wiener filtering of the projections. Nucl. Instrum. Meth. A 423, 265–271 (1999).

[10] Mäkitalo, M., Foi, A. “Optimal inversion of the Anscombe transformation in low-count Poisson image denoising”, IEEE T Image Process. 20(1), 99-109 (2011).
[11] Rabbani, M. “Bayesian filtering of Poisson noise using local statistics”, IEEE T. Acoust. Speech 36(6), 933-937, (1998).
[12] Pokrajac, D. D., Maidment, A. D. A., Bakic, P. R. “Optimized generation of high resolution breast anthropomorphic software phantoms” Med. Phys. 39(4), 2290-2302 (2012).
[13] Bakic, P. R., Zhang, C., Maidment, A. D. A. “Development and characterization of an anthropomorphic breast software phantom based upon region-growing algorithm”. Med. Phys. 38(6), 3165-3176 (2011).
[14] Bakic, P. R., Ng S., Ringer, P., Carton, A-K., Conant, E. F., Maidment, A. D. A. “Validation and optimization of digital breast tomosynthesis reconstruction using an anthropomorphic software breast phantom” Proc. SPIE 7622, 76220F (2010).
[15] Ruiter, N. V., Zhang, C., Bakic, P. R., Carton, A-K., Kuo, J., Maidment, A. D. A. “Simulation of tomosynthesis images based on an anthropomorphic software breast tissue phantom”. Proc. SPIE 6918, 69182I (2008).
[16] Zhang, C., Bakic, P. R., Maidment, A. D. A. “Development of an Anthropomorphic Breast Software Phantom Based on Region Growing Algorithm” Proc. SPIE 6918, 69180V (2008).
[17] Wang, Z. and Bovik, A. C. “Mean squared error: Love it or leave it? A new look at signal fidelity measures”. IEEE Signal Proc. Mag. 26(1), 98-117 (2009).
[18] Wang, Z., Bovik, A. C., Sheikh, H. R., Simoncelli, E.P. “Image quality assessment: from error visibility to structural similarity”. IEEE T Image Process. 13(4), 600-612 (2004).
[19] Kuo J., Ringer P. A., Fallows S. G., Bakic P. R., Maidment A. D. A., Ng S. “Dynamic reconstruction and rendering of 3D tomosynthesis images,” Proc. SPIE 7961, 796116 (2011).